X-RAY MICROSCOPY WITH SYNCHROTRON RADIATION AND 3-DIMENSIONAL IMAGE DATA PROCESSING

Lotti JOCHUM and Bastian NIEMANN

Forschungseinrichtung Röntgenphysik, Universität Göttingen, Geiststraße 11, 3400 Göttingen, Fed. Rep. of Germany

Key words: X-ray microscopes, X-ray lenses, Contrast mechanisms, X-ray sources, Image Processing

Abstract.   In the last decade research with soft x-rays has regained importance, because improved laboratory technology allowed to build high quality focusing and dispersing optics. This progress made new research possible such as x-ray microscopy. In addition intense soft x-ray sources were developed, e.g. storage rings, undulators and plasma sources which overcome the handicap of too little x-ray flux in earlier times. In the field of x-ray microscopy the development has resulted in instruments which can be applied to many biological, medical and physical fields; the most outstanding challenge is to examine living cells in a wet state at air pressure. First attempts have been made to examine the 3-dimensional structure of specimen. In this paper some aspects important for the concept of x-ray microscopy and experimental results are presented.

1.   CONTRAST MECHANISM

The interaction of x-radiation with matter can in general be described by elastic and inelastic processes. In the ultrasoft x-ray region two kinds of interaction are dominant: coherent scattering, which leads to phase shifting of the x-radiation, and absorption, which, according to the Huygens—Fresnel principle, generates a diffracted wave without phase information. This is described by the complex refracting index:

$$n = 1 - \delta - i\beta \tag{1}$$

with:
$$\delta = \frac{r_0 \times \lambda^2}{2\pi} \, N \times f_1 \tag{2a}$$

and
$$\beta = \frac{r_0 \times \lambda^2}{2\pi} N \times f_2 \tag{2b}$$

$f = f_1 + if_2 =$ atomic scattering factor, $r_0 =$ electron radius, $\lambda =$ wavelength, $N =$ number of atoms per cm^3; f_1, f_2 is tabulated e.g. in HENKE (1981). The amplitude transmission T of an object of the thickness t is given by:

$$T = A_1/A_0 = \exp\left\{ -\frac{2\pi i}{\lambda} n \times t \right\} \tag{3}$$

$A_0 =$ complex amplitude of the incident wave
$A_1 =$ complex amplitude of the transmitted wave
$t =$ thickness of the matter.
Combining Eq. (1) and Eq. (3) leads to:

$$T = \exp\left\{ -\frac{2\pi}{\lambda} \beta \times t \right\} \times \exp\left\{ \frac{2\pi i}{\lambda} \delta \times t \right\} \times \exp\left\{ -\frac{2\pi i}{\lambda} t \right\}. \tag{4}$$

The first term represents the photoelectric absorption of the x-radiation, where $(2\pi/\lambda) \times \beta =: \mu$ is the linear absorption coefficient of the regarded material. The second term represents the phase shift of the transmitted wave with respect to the phase in vacuum, which is given by the third term.

1.1 Amplitude contrast and phase contrast

X-ray microscopes, working in the amplitude contrast mode, are sensitive to the absorption of photons in the object, whereas in the phase contrast mode the phase shift, which is related to the coherent scattering of photons, contributes to the phase contrast mechanism. The contrast mechanism which leads to amplitude contrast in the soft x-ray region is illustrated in Fig. 1.

It shows the linear absorption coefficient as a function of the wavelength for different materials. Between $\lambda = 2.3$ nm and $\lambda = 4.4$ nm there is about one order of magnitude difference between the absorption coefficients of water and organic components, as e.g. proteins. This difference provides a natural contrast mechanism for the investigation of biological material. However, it is difficult to realize instruments working purely in one single mode, if very high resolution x-ray optics are used. The reason for this is quite simple. As the object thickness exceeds the focal depth of the objective in general (see paragraphs 2.2 and 3.1), there are always in-focus and out-of-focus object regions. The in-focus plane will show amplitude contrast, defocussed object layers show phase contrast. In the phase contrast mode this situation is reversed. In addition, it is impossible to realize phase plates for soft x-rays which have no absorption. This gives a further reason why the pure phase contrast mode can not be realized. Nevertheless, for thin samples it can be nearly approximated and it is planned to develop an instrument for this purpose.

The image contrast and the dosage transferred to the object have been calculated for the ideal phase contrast microscope and is shown in comparison to the pure amplitude contrast mode in Fig. 2a–b. The absolute number refers to 100%
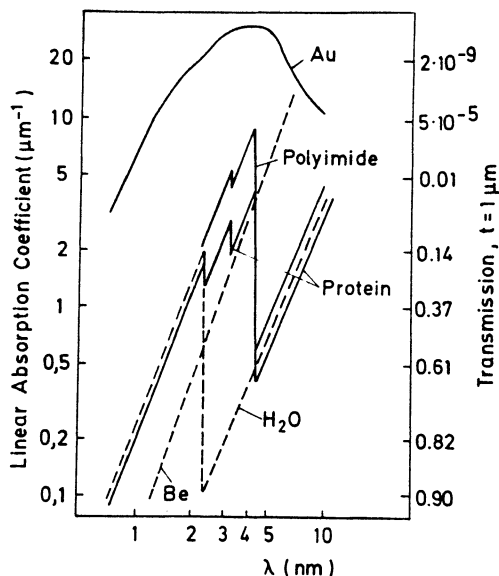
Fig. 1.   Linear absorption coefficient for various materials.

efficient optics and detectors (Rudolph *et al.*, 1989). It can been seen that even in the wavelength range below the water window the phase contrast is higher at a lower dose than the amplitude contrast in the water window.

2.   X-RAY OPTICS

Imaging optics can in general be based on the principle of refraction, reflection or diffraction. As for soft x-rays the linear absorption coefficient is in the range of $0.1...10 \, \mu m^{-1}$, one could only construct very thin refraction lenses and their effective diameter is limited to some $10 \, \mu m$. As the real part of the refracting index is only a little bit smaller than 1, one could only construct a concave focusing lens with a long focal length. The small effective diameter and the long focal length result in a low diffraction limited resolution. For this reason refracting optics can not be used.

2.1   Reflecting optics
2.1.1   Grazing incidence optics
As the real part of the refracting index is lower than 1, reflecting optics can be realized for total reflection; such optics use grazing incidence angles up to a few degrees. The precision requirements in the fabrication of grazing incidence optics are very high (Franks *et al.*, 1984). The surface roughness has to be in the order of 1 nm to get a sufficient reflectivity and the precision of the surface shape has to be in the same range. Such systems are mainly used for diagnostics of hot plasmas and in x-ray astronomy. As the focal length is independent of the wavelength, such optics can be used to focus a broad wavelength range at the same time.
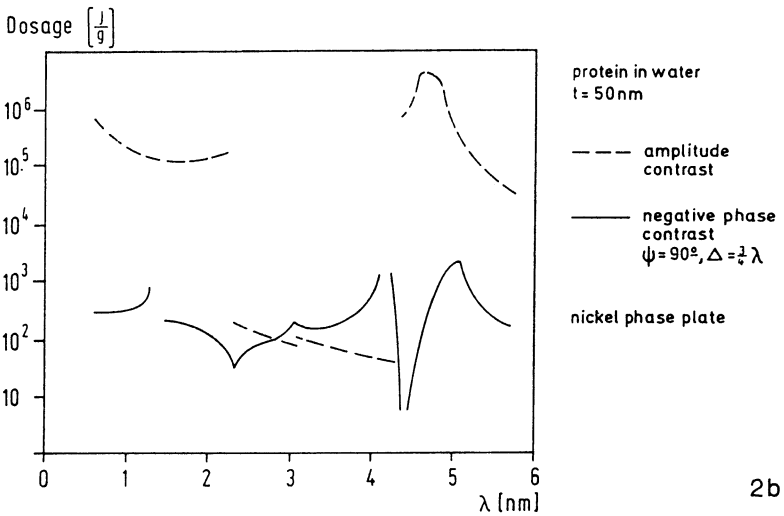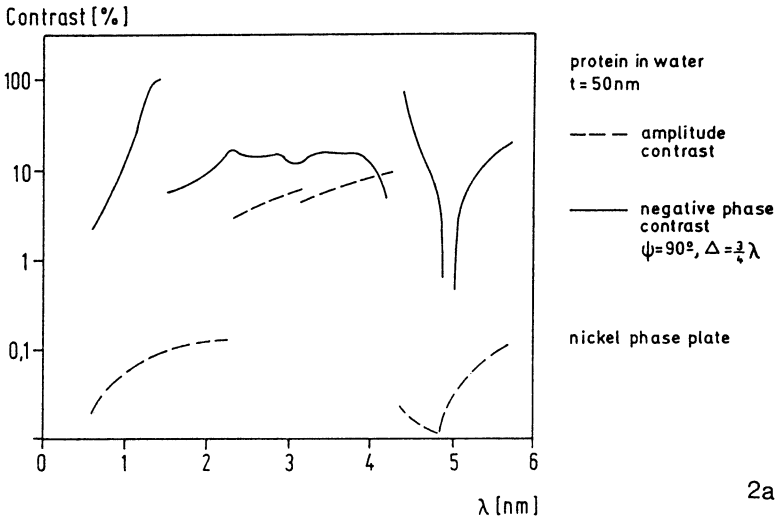
Contrast [%]

protein in water
t = 50 nm

– – – amplitude
contrast

——— negative phase
contrast
$\psi = 90°, \Delta = \frac{3}{4}\lambda$

nickel phase plate

2a

Dosage $\left[\frac{J}{g}\right]$

protein in water
t = 50 nm

– – – amplitude
contrast

——— negative phase
contrast
$\psi = 90°, \Delta = \frac{1}{4}\lambda$

nickel phase plate

2b

Fig. 2a–b.   Image contrast (a) and the dosage transferred to the object (b) for amplitude- and negative phase contrast.

2.1.2   Normal incidence optics

According to the Fresnel formula the reflectivity for normal incidence is proportional to:

$$R \sim \delta^2 + \beta^2 \tag{5}$$

with δ and β as given in Eqs. (2a) and (2b). For soft x-rays, R is the order of 10^{-6}.

The reflectivity can be increased considerably by use of multilayer coatings consisting of relatively transparent (low z) materials as e.g. carbon, alternating with thin reflecting (high z) layers of e.g. ReW alloy. The thickness of the layers has to be approximately one quarter of the wavelength so that all reflected waves can interfere constructively. If a broad wavelength range meets a multilayer optic, only a narrow wavelength range interferes constructively and is reflected with a high reflectivity; values above 10% have been achieved (Dhez, 1984; Barbee, 1984). Designs of spherical mirrors with multilayer coatings and a resolution of 1 arc second in the 17 nm wavelength region are made and have successfully been applied in x-ray astronomy (Walker et al., 1988). In x-ray microscopy applications a resolution in the 1 μm range was achieved (Haelbich et al., 1980).

2.2   Diffraction optics

Diffraction optics are well suited to image x-rays, they can deliver high spatial resolution. A special type of diffraction optics are the Fresnel zone plates. Zone plates are circular symmetrical gratings with radially increasing line density (see Fig. 3). They are widely used as diffraction lenses in x-ray microscopy.

Soret (1875) discussed the properties of zone plates more than one hundred years ago. It is now well established that imaging with zone plates of zone numbers $n>100$ obeys the same laws as does imaging with refracting lenses. With r_1=radius of the innermost zone, r_n=radius of the n-th zone, n=zone number and m= diffracted order, the focal length of a zone plate is approximately given by:

$$f_m = r_1^2 \times \lambda^{-1} \times m^{-1}. \tag{6}$$

The width of the outermost zone is $dr_n=r_n/(2n)$. According to the Rayleigh criterion the transverse resolution of a zone plate is:

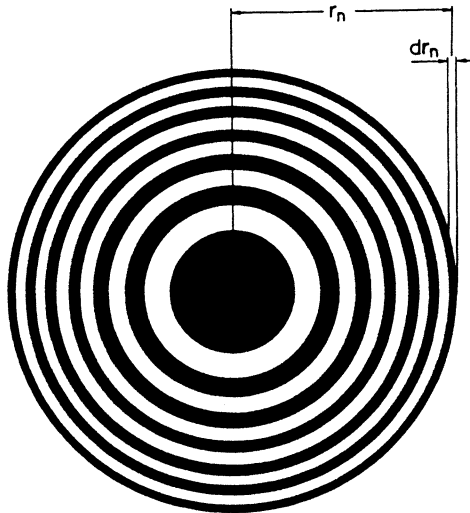Fig. 3.   Zone plate structure.

$$d_t = 1.22 \, \frac{dr_n}{m} \, . \tag{7}$$

The geometric optical depth resolution of a zone plate is given by:

$$d_d = 0.61 \, \frac{r_1^4}{r_n^2 \times \lambda} \, . \tag{8}$$

The maximum diffraction efficiency of amplitude zone plates, which consist of non absorbing zones alternating with totally absorbing zones, is theoretically 10% in the first diffraction order, whereas 5–7% are already good values in practice. To improve the efficiency to a value above 10% one can use phase zone plates which contain phase shifting zones instead of the totally absorbing zones. For symmetrical zone profiles efficiency values of 40% in the first diffraction order are theoretically possible. As each phase shifting material absorbs the radiation remarkably in practice the attainable efficiency is limited to about 20–30%. Phase zone plates can also be realized advantageously at shorter wavelengths where f_2, which is related to the absorption, decreases in general, whereas f_1, which is related to the phase shift, approaches z, the atomic number of the regarded material. As $f_m \sim 1/\lambda$ (see Eq. 6), a zone plate has to be used with quasi- monochromatic radiation with a bandwidth of $\Delta\lambda/\lambda = 1/(n \times m)$ to avoid chromatic aberrations. In this case a monochromator must preced the zone plate.

3. ZONE PLATE FABRICATION

As the resolution of zone plates for soft x-rays is related to the outermost zone width (see Eq. (7)), fabrication methods which deliver submicron zone widths must be used. The holographic method and the electron beam writing are in current use. Two further methods are proposed and/or in an experimental state: x-ray interference and the "sputtered sliced zone plate" (SSZP) method.

3.1 Holographic zone plate fabrication

A zone plate pattern is a hologram of a point source. It can be generated by the superposition of a spherical wavefront with a reference wavefront, which can be a plane or a spherical wavefront. These two waves interfere and the system of alternating bright and dark interference fringes which occurs is a zone plate structure. This structure can be recorded with a photoresist layer and can be processed with lithographic methods into a metal zone plate, as described in 3.2.

In our laboratory UV laser-light generates the interference pattern. It is well known that a hologram has to be reconstructed with the same wavelength and under the same geometrical conditions as used for construction, otherwise strong aberrations occur. Therefore the UV-wavefronts are generated with large aberrations by specially designed optical systems to compensate aberrations when reconstructing the source point with x-rays. Detailed descriptions of this method as well as of the optical systems and parameters of various zone plates are given in Schmahl et al. (1984). Micro zone plates of the type MZP3 with 60 nm diffraction limited

transverse resolution and 1.69 μm focal depth resolution as well as condenser zone plates of the type KZP3 with 15000 zones at 9 mm diameter are examples of holographically fabricated zone plates which are in current use at the Göttingen x-ray microscope.

3.2 Electron beam writing

This technique is an application of the electron beam lithography. The zones are written by a moving electron beam on an electron sensitive resist. The developed resist acts as a mask. This zone plate pattern is then transferred into absorbing or phase shifting materials by means of ion milling or a combination of reactive ion etching and ion milling. It is also possible to fill up the resist structures by electroplating. Electron beam written micro zone plates are fabricated by IBM, USA (Vladimirsky *et al.*, 1986), Institut für Halbleitertechnik, Aachen (Bögli *et al.*, 1988), Kings College (Buckley *et al.*, 1988) and Osaka University, Japan (Aritome *et al.*, 1987).

The electron beam written zone plate ZP40 with 40 nm outermost zone width has been fabricated by Y. Vladimirsky and was tested successfully in our x-ray microscope (Vladimirsky *et al.*, 1989).

Nevertheless, as with this method the zones are written point by point, it is not very useful for the fabrication of condenser zone plates with very high zone numbers, because the necessary writing time is in the range of days, which must be compared with an exposure time of some 10 seconds when using the holographic method.

3.3 X-ray Interferometric zone plates

Using an x-ray zone plate itself as an x-ray interferometer by illuminating it with spatially coherent, quasimonochromatic x-radiation, the superimposed first and second order radiation yields an x-ray interference figure which again has structures of a zone plate. This structure has to be converted into metal zones by use of x-ray lithographical methods. The illuminating source must have a high spectral brilliance, e.g. a high photon flux within a small bandwidth from a small source size and a low x-ray beam divergence. This can be achieved with an undulator at a storage ring. A holographically fabricated zone plate (MZP3) has been developed in Göttingen (Schmahl *et al.*, 1984) which can be used as an x-ray interferometer. It would deliver a zone plate pattern with 20 nm outermost zone widths (MZP4).

3.4 Sputtered sliced zone plates

To get zone plates for a resolution range of $10 \leq d \leq 50$ nm a method is being developed to make sputtered sliced zone plates (Rudolph *et al.*, 1982; Bionta *et al.*, 1988). To produce such zone plates, layers of an opaque or a phase shifting and a highly transparent material are deposited alternatingly onto a thin wire. Then the wire is sliced perpendicular to its axis; the slices are ring zone plates and the core wire acts as a central stop. This technique can produce zone plates with a high aspect ratio. It is therefore advantageously applicable to phase zone plates, as the zones can be made thick enough, about some 100 nm, to produce sufficient phase shifts. This is especially useful for zone plates working at wavelengths in the nm range.

4. X-RAY SOURCES FOR MICROSCOPY

Early attempts to produce microscopic shadow images were done with conventional x-ray tubes using characteristic K-radiation or Bremsstrahlung (Cosslett *et al.*, 1951, 1961). In order to get a short exposure time for microscopic images it is generally necessary to use sources with a high power N/sec and at a low emittance $\Omega \times F$. Herein N/sec is the number of photons emitted per sec, F is the photon emitting area and Ω is the solid angle of the radiation cone. Diffraction lenses and multilayer optics as imaging elements have to be illuminated with radiation of a narrow bandwidth $BW = \Delta\lambda/\lambda$. Thus the spectral brilliance SB, given by:

$$SB = N/(F \times \Omega \times BW \times \text{sec}) \tag{9}$$

is the relevant physical quantity when comparing different x-ray sources; it has to be as high as possible.

4.1 Synchrotron radiation

Soft x-rays, suited for x-ray microscopy, are generated by bending magnets of synchrotrons and of storage rings, by undulators and plasma sources. Soft x-ray lasers are under development.

Synchrotrons were introduced more than 20 years ago. Their SB is at least 6–8 orders of magnitude higher than that of conventional x-ray tubes. The development of storage rings leads to another increase in the SB of 1–2 orders of magnitude. They are now generally used for x-ray microscopy work.

Synchrotrons and storage rings deliver dipole radiation from relativistic electrons in a bending magnet which shows a continuous spectrum to the microscope. Undulators contain a multipole magnet arrangement, which produces interference effects in the emitted radiation field. They deliver discrete (harmonic) wavelengths with an increased spectral brilliance. As undulators emit discrete wavelengths, it is possible to construct devices which deliver the same total input flux to the microscopes as does the continuous spectrum from a bending magnet, but which can have a spectral brilliance which is an order of magnitude higher than that from a bending magnet. This can be important, because the maximum power, which may be exposed to the first optical element in the beam without degrading its performance, is in general limited.

Plasma focus sources are compact and are suited for "single user" laboratories. They deliver the x-ray photons in short pulses of nanosecond duration and show a multiple line spectrum; by tuning the parameters of the source the flux into a single line can be optimized, additional filtering of undesired wavelength components can be necessary.

Such a source is operated at the Göttingen laboratory microscope (Neff *et al.*, 1988; Niemann *et al.*, 1990). The expected time averaged spectral brilliance is still less than that achievable at storage rings. Nevertheless, if the flux produced by a single pulse becomes high enough so that an x-ray image can be recorded with sufficient resolution and signal to noise ratio, such a source overcomes the handicap

of blurring the image by motions of living specimens.

5.   X-RAY MICROSCOPES

The prototype of a sub-micron resolution imaging x-ray microscope (XM) was established and run in 1976 at "Deutsches Elektronensynchrotron DESY" (Niemann *et al.*, 1976). 1978 an improved microscope was installed at the electron storage ring ACO in Orsay and is now operating at the BESSY storage ring in Berlin.

The development of scanning x-ray microscopes (SXM) which use zone plates as focusing optics was started about 10 years ago by several groups (Kirz *et al.*, 1980; Niemann *et al.*, 1982; Niemann, 1984; Duke, 1984).

5.1   *The Göttingen x-ray microscope*
Figure 4 shows the optical arrangement in a zone plate x-ray microscope (XM).
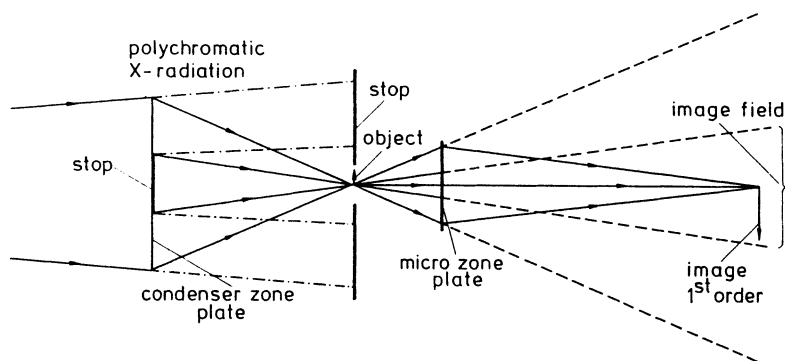
Fig. 4.   Schematic outline of the Göttingen x-ray microscope (XM).

The microscope contains a monochromatic object illumination and an imaging part. The polychromatic synchrotron radiation illuminates the condenser zone plate which produces a demagnified image of the synchrotron source. A diaphragm is adjusted to the image spot. This arrangement of the condenser and the diaphragm acts as a linear monochromator and illuminates the object. An enlarged image of the object is produced by the micro zone plate. To operate the micro zone plate with its maximum possible spatial resolution, the bandwidth of the illuminating radiation has to be $\Delta\lambda/\lambda = 1/(n \times m)$. This spectral resolution can be obtained by choosing appropriate monochromator dimensions. The magnified image can be seen on an x-ray-to-visible converter (a channel plate with phosphor screen) directly, or a movable camera, placed in the evacuated microscope, takes a photograph of the real x-ray image. Radiation of the zero order of the condenser zone plate would reduce the contrast of the x-ray image but a circular stop placed concentric to the center of the condenser zone plate avoids this (see Fig. 4). Thus, no zero order radiation of the condenser zone plate illuminates and passes the object. Consequently the image plane is free from zero order radiation of the condenser zone plate.

Only first order radiation from the condenser meets the object and is diffracted by the object into different orders. The light of each diffraction order of the object is again diffracted by the micro zone plate into many orders. All first order radiation of the micro zone plate forms the image in the image plane. All other order radiation of the micro zone plate does not contribute to the image, it merely contributes to the background superimposed to the image.

The background is very strong outside the image field. Here mainly the radiation occurs, which is undiffracted by the object and undiffracted by the micro zone plate. Without the central stop on the condenser zone plate this undiffracted radiation would also fill up the central image field. Figure 5 shows an image which has been recorded at the Göttingen XM using MZP3 with $\lambda=4.5$ nm (Nyakatura *et al.*, 1988).
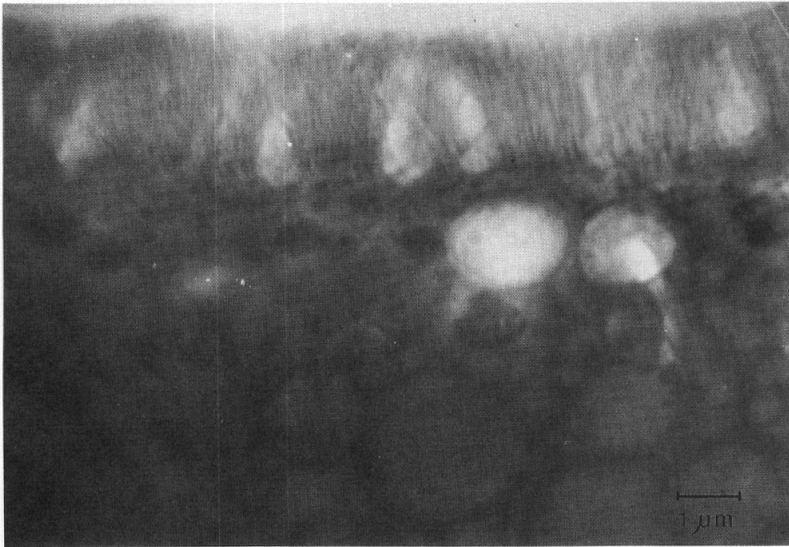
Fig. 5.   Section of renal procximal tubule of the rat.

The x-ray microscope can also be used in the phase contrast mode, as described in 2.2, by introducing a phase plate in the back focal plane of the microscope (Zernike, 1935) as shown in Fig. 6.

Figure 7 shows an x-ray image, recorded with the phase contrast arrangement shown in Fig. 6, with a silver phase plate of 120 nm thickness. The exposure time was 30 s at an electron beam current of 240 mA.

The phase plate in Fig. 6 only affects the phase of the high spatial frequency components in the object spectrum because the illumination is only partially coherent. This can be altered with special condenser arrangements as shown in Fig. 8. Figures 6, 7 and 8 are taken from Schmahl *et al.*, 1988.
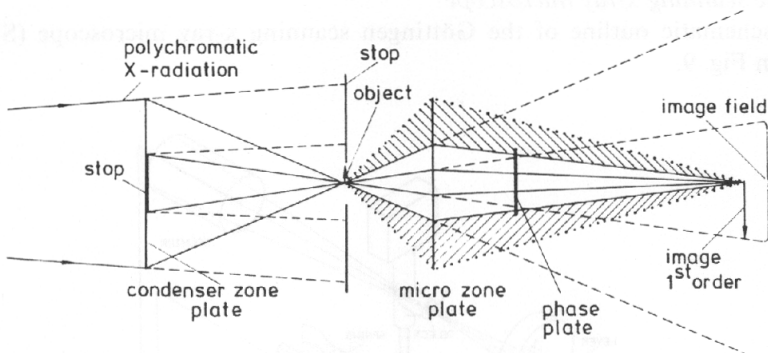
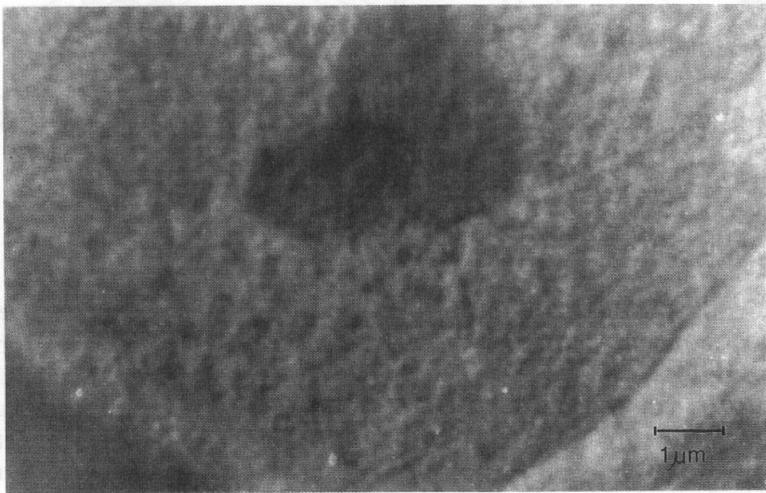Fig. 6. Phase contrast x-ray microscope with partially coherent illumination.

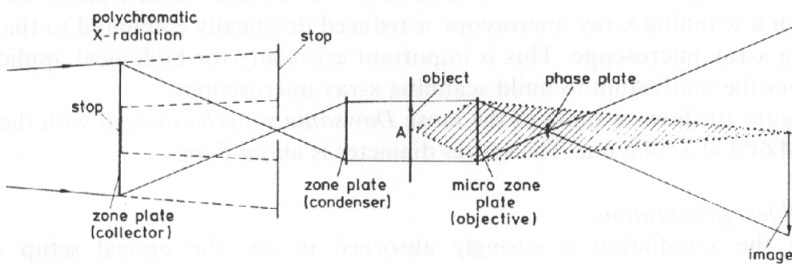Fig. 7. Part of a necleus of a human fibroplast imaged with phase contrast.

Fig. 8. Phase contrast x-ray microscope with quasicoherent illumination.

5.2 The scanning x-ray microscope

A schematic outline of the Göttingen scanning x-ray microscope (SXM) is shown in Fig. 9.
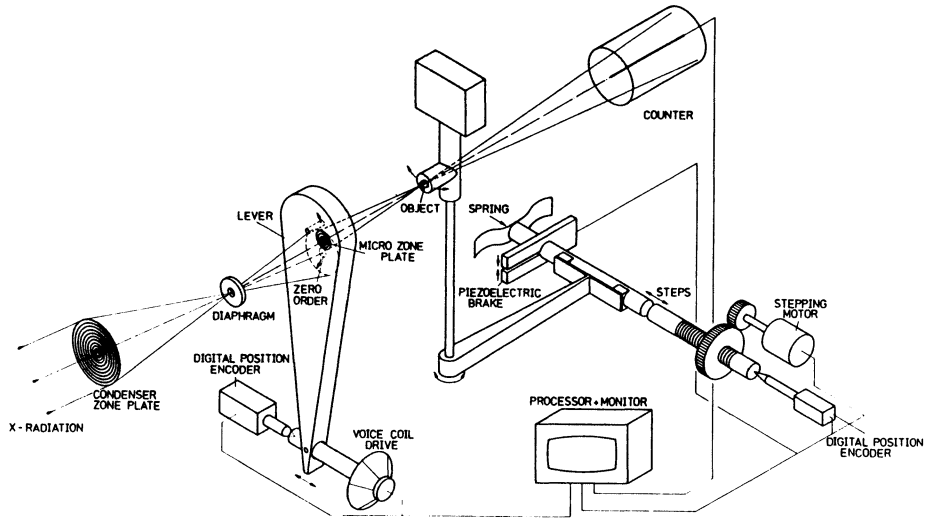
COUNTER

LEVER
OBJECT SPRING
MICRO ZONE PLATE
ZERO ORDER
DIAPHRAGM
PIEZOELECTRIC BRAKE STEPS STEPPING MOTOR
DIGITAL POSITION ENCODER
CONDENSER ZONE PLATE
X - RADIATION
PROCESSOR + MONITOR
VOICE COIL DRIVE
DIGITAL POSITION ENCODER

Fig. 9. Schematic outline of the Göttingen scanning x-ray microscope (SXM).

The optical setup within the microscope consists of two stages: a linear zone plate monochromator, in which a condenser zone plate focuses the synchrotron light through a small diaphragm, and a micro zone plate which images the diaphragm to the ultimate scanning spot size of 60 nm (diffraction limited). This spot scans the object and the transmitted light will be measured by a high efficient x-ray detector; a real time image will be build up on a TV-monitor. As an x-ray detector, gas proportional counters can be used with a detective quantum efficiency of 50% or more. Between the object and the detector there is no loss of photons. This is different to an imaging x-ray microscope where a low efficient micro zone plate is between the object and the detecting device. The radiation dose transferred to the object in a scanning x-ray microscope is reduced drastically compared to that in an imaging x-ray microscope. This is important especially for biological applications and gives the motivation to build scanning x-ray microscopes.

Figure 10 shows a spore of the moss *Dawsonia superba* imaged with the SXM using MZP3 at $\lambda=4.5$ nm. The spores diameter is about 5 μm.

5.3 Object preparation

As the x-radiation is strongly absorbed in air, the optical setup of the microscope is situated in vacuum vessels. Observing a wet object, only the object is located in a small chamber which can be filled with air and is closed vacuum tight by two low absorbing foils. A schematic of such a chamber for the XM is shown in Fig. 11.
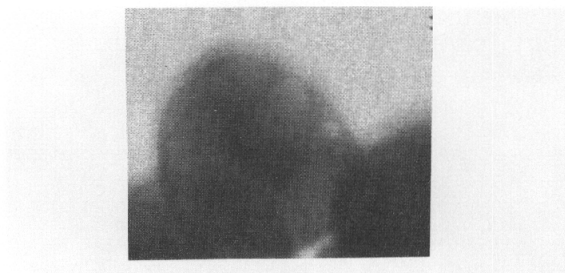
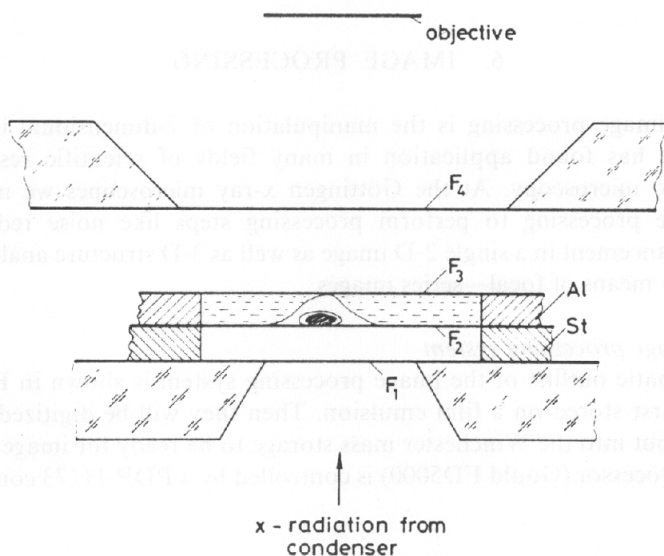Fig. 10. SXM image: Spore of the moss *Dawsonia superba*.

Fig. 11. Schematic arrangement of the environmental chamber (not to sale)

The regions outside the foils F1 and F4 are evacuated. The small volume between foils F1 and F2 and the space between F3 and F4 can be pumped down to a pressure of about 300 mbar. The small volume between the foils F2 and F3 contains the object surrounded by physiological saline solution.

As the linear absorption coefficient of water is in the order of 1 μm^{-1} for soft x-rays, only very thin water layers of a few μm can be tolerated. One of the main difficulties, when examining wet material, is to keep the water layer thin enough and to prevent drying. Otherwise the osmotic pressure changes and crystal growth arises; this can destroy the biological specimen.

Figure 12 shows an x-ray image of a wet FES cell. The exposuretime was 60 sec with a ring current of 400 mA (Nyakatura *et al.*, 1988).
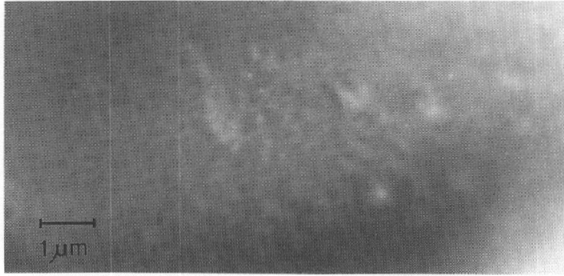
Fig. 12.   Part of a wet FES cell imaged with MZP3 at $\lambda=4.5$ nm.

6.   IMAGE PROCESSING

Digital image processing is the manipulation of 2-dimensional images by a computer. It has found application in many fields of scientific research from astronomy to microscopy. At the Göttingen x-ray microscopes we make use of digital image processing to perform processing steps like noise reduction and contrast enhancement in a single 2-D image as well as 3-D structure analysis of thick specimens by means of focal—series images.

6.1   The image processing system

A schematic outline of the image processing system is shown in Fig. 13. The images are first stored on a film emulsion. Then they will be digitized by a CCD camera and put into the Winchester mass storage to be ready for image processing. The image processor (Gould FD5000) is controlled by a PDP-11/73 computer. The
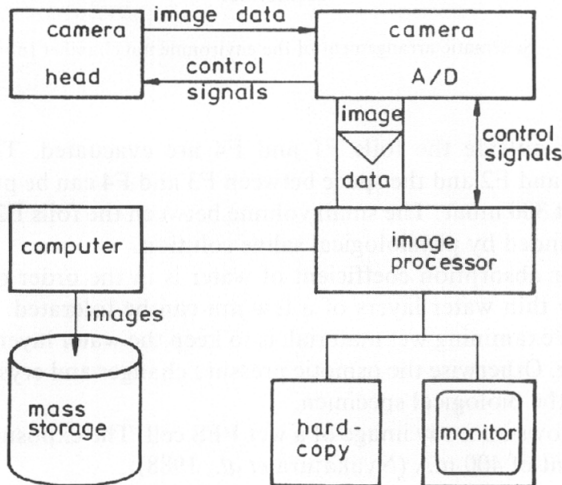

Fig. 13.   CCD camera and image processing system.

images can be displayed on a color TV-monitor and a hardcopy unit enables us to get slides or prints of the processed images.

6.2 3-D structure analysis

X-ray microscopy enables us to investigate specimens which are thick compared to the focal depth of the imaging system. It is obvious that the 3-D structure and the orientation or location of substructures can not be fixed in one single image. Therefore, the object volume has to be sampled slice by slice to get the full 3-D information. After having sampled the object volume, the 3-D structure of the object can be visualized by image processing methods.

At the Göttingen x-ray microscope such experiments have been made with cotton strings as a test object. The cotton strings were placed in the object chamber of the XM and a set of focal series images at 33 different z-positions (z-direction=optical axis) were recorded with a distance of 1 μm from plane to plane using MZP3 at $\lambda=4.5$ nm. The resolution is 60 nm perpendicular to the optical axis, which is the x-y-plane; the geometric optical depth resolution is 1.69 μm. From the focal series images crosscuts of different object planes parallel to the optical axis were calculated. On these crosscuts one can see the depth structure of the cotton strings in the actually chosen object plane.

Three focal series images are shown in Fig. 14a–c. The magnification, when recording in the x-ray microscope, was 300 times. The images were first stored on a
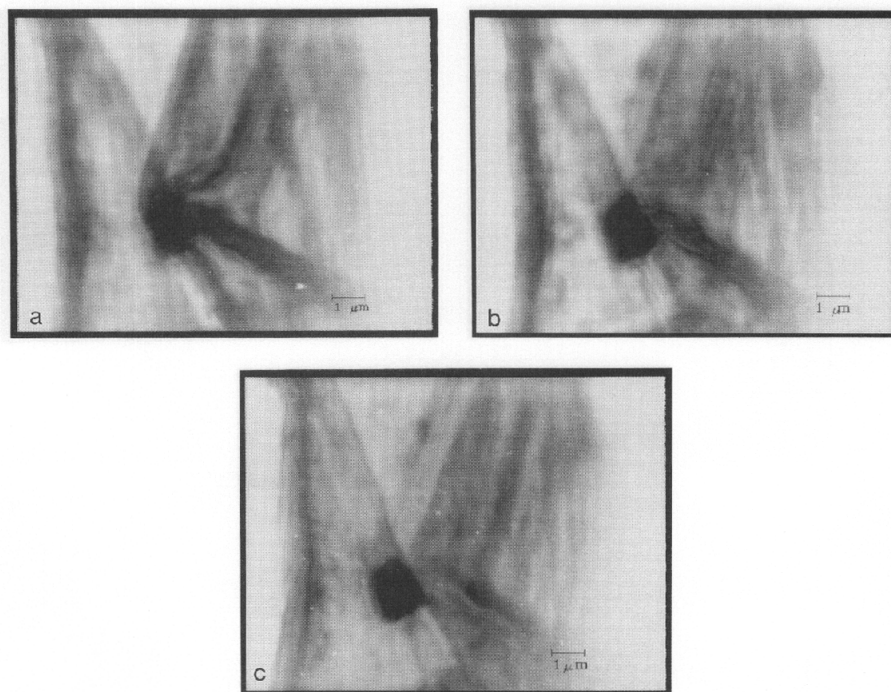

Fig. 14a–c. Focal series images. 14a: $z=3$, 14b: $z=14$, 14c: $z=30$.

film emulsion and then digitized through a Zeiss microscope by a CCD camera. The total magnification is 375 times. The images are median filtered to reduce the noise.

One can see, as expected, that the appearance of the object changes drastically from plane to plane.

Figure 15 shows one of the focal series images; the three x-positions at which the z-y-cuts have been calculated are drawn in. They are 25 pixels distant from each other. This corresponds to a distance in the object of about 0.6 μm.
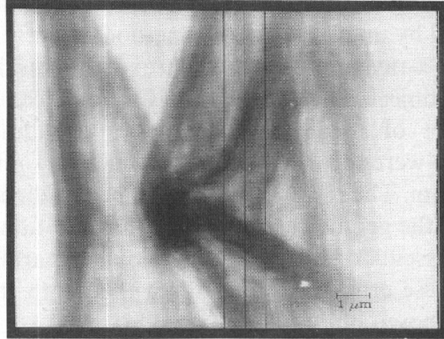

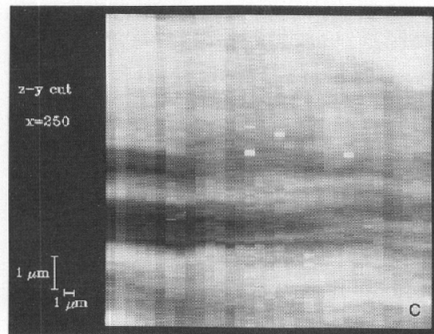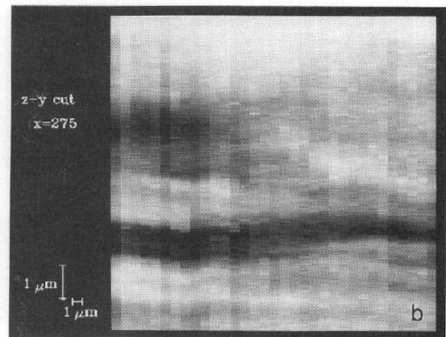Fig. 15.   Positions of the z-y-cuts which are shown in Fig. 16a–c; $x=300$; 275; 250 from right to left.
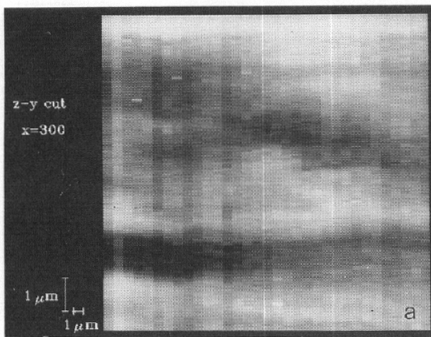

Fig 16a–c. z-y-cuts at different x-positions.

The three calculated z-y-cuts are shown in Fig. 16a–c. The elliptical structures correspond to the crosscuts through the cotton strings in Fig. 15, which are intersected by the vertical line. A focusing through the object volume from the left to the right can be simulated by looking at several z-y-cuts sequentially.

In Figure 17 one can see the y-positions at which the z-x-cuts have been calculated. The resulting images are shown in Fig. 18a–b.

The depth structure of the cotton strings, which can be estimated by looking at all the focal series images sequentially, can be seen in one single view for a fixed x- or y-position. This gives very helpful information when trying to construct a model of the objects shape.
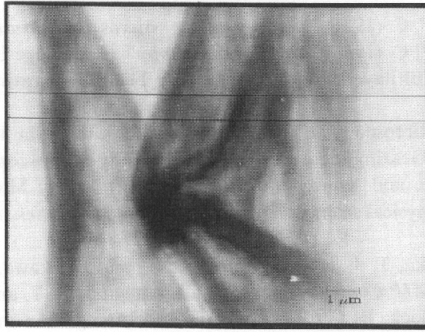

Fig. 17. y-positions of the z-x-cuts which are shown in Fig. 18a–b. $y=341$ (upper one), $y=311$ (lower one).
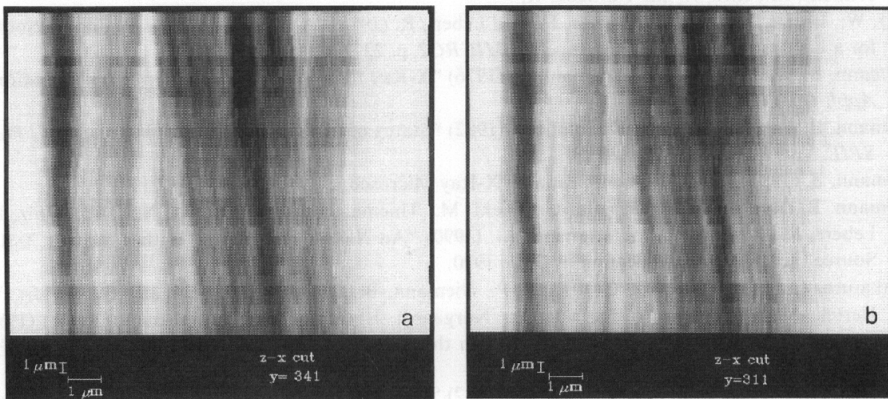

Fig. 18a–b. z-x-cuts at different y-positions.

Acknowledgements

132

REFERENCES

Aritome, H. and Namba, S. (1987) "Fabrication of X-Ray Optical Elements by Electron Beam Lithography" in *SPIE Proc.* **733**, p.440–448.

Barbee, T. W. (1984) "Multilayers for X-Ray Optical Applications" in *MICRO1*, p. 144–162.

Bionta, R. M., Jankowski, A. F., and Makowiecki, D. M. (1988) "Sputtered-Sliced Linear Zone Plates for 8 keV X-Rays" in *MICRO2*, p. 142–145.

Bögli, V., Unger, P., Beneking, H., Greinke, B., Guttmann, P., Niemann, B., Rudolph, D., and Schmahl, G. (1988) "Microzone Plate Fabrication by 100 keV Electron Beam Lithography" in *MICRO2*, p. 80–87.

Buckley, C. J., Browne, M. T., Burge, R. E., Charalambous, P., Ogawa, K., and Takeyoshi, T. (1988) "Zone Plates for Scanning X-Ray Microscopy: Contamination Writing and Efficiency Enhancement" in *MICRO2*, P. 88–94.

Cosslett, V. E. and Nixon, W. C. (1951) "X-Ray Shadow Microscope", *Nature*, Vol. **168**, p. 24.

Cosslett, V. E. and Nixon, W. C. (1961) "*X-Ray Microscopy*", Cambridge Univ., Press, London.

Dhez, P. (1984) "Use of Multilayers for X-UV Optics: Their Fabrication and Tests in France" in *MICRO1*, p. 139–143.

Duke, P. J. (1984) "X-Ray Microscopy at The Daresbury Laboratory", in *MICRO1*, p. 232–241.

Franks, A., Gale, B. (1984) "Grazing Incidence Optics for X-Ray Microscopy" in *MICRO1*, p. 129–138.

Haelbich, R. P., Staehr, W., and Kunz, C. (1980) "Ultrasoft X-Ray Microscopy: its application to biological science and physical sciences", in *Ann. of NY Acad. of Sci.*, ed. Parsons, D. F., Vol. **342**, p. 148–157.

Henke, B. L., Lee, P., Tanaka, T. J., Shimabukuro, R. L., and Fujikawa, B. K. (1981) "Low Energy X-Ray Diagnostics", in *AIP Conf. Proc.* No 75, eds. Attwood, D. T. and Henke, B. L., p. 340–388.

Kirz, J., Burg, R., and Rarback, H. (1980) "Plans for a Scanning Transmission X-Ray Microscope", *Ann. of NY Acad. of Sci.*, ed. Parsons, D. F., Vol. **342**, p. 135–148.

Micro1 (1984): "X-Ray Microscopy", *Springer Series in Optical Sciences*, Vol. **43**, eds. Schmahl, G. and Rudolph, D.

Micro2 (1988): "X-Ray Microscopy II", *Springer Series in Optical Sciences*, Vol. **56**, eds. Sayre, D., Howells, M., Kirz, J., and Rarback, H.

Neff, W., Eberle, J., Holz, R., Richter, F., and Lebert, R. (1988) "A Plasma Focus as Radiation Source for a Laboratory X-Ray Microscope" in *MICRO2*, p. 22–29.

Niemann, B., Rudolph, D., and Schmahl, G. (1976) "X-Ray Microscopy with Synchrotron Radiation", *Appl. Opt.* Vol. **15**, p. 1883.

Niemann, B., Schmahl, G., and Rudolph, D. (1982) "Status of the Scanning X-Ray Microscope", *Proc. SPIE*, Vol. **316**, p. 106–108.

Niemann, B. (1984) "The Göttingen Scanning X-Ray Microscope", in *MICRO1*, p. 217–225.

Niemann, B., Rudolph, D., Schmahl, G., Diehl, M., Thieme, J., Meyer-Ilse, W., Neff, W., Holz, R., Lebert, R., Richter, F., and Herziger, G. (1990) "An X-Ray Microscope With a Plasma X-Ray Source" accepted for publication in Optic 1990.

Nyakatura, G., Meyer-Ilse, W., Guttmann, P., Niemann, B., Rudolph, D., Schmahl, G., Sarafis, V., Hertel, N., Uggerhøj, E., Skriver, E., Nørgaard, J. O. R., and Maunsbach, A. B. (1988) "Investigations of Biological Specimens with the X-Ray Microscope at BESSY", in Micro 2, p. 365–371.

Rudolph, D., Niemann, B., and Schmahl, G. (1982) "Status of the Sputtered Sliced Zone Plates" *Proc. SPIE*, Vol. **316**, p. 103–105.

Rudolph, D., Schmahl, G., and Niemann, B. (1989) "Amplitude and Phase Contrast in X-Ray Microscopy" to be published.

Schmahl, G., Rudolph, D., Guttmann, P., and Christ, O. (1984) "Zone Plates for X-Ray Microscopy" in *MICRO1*, p. 63–74.

Schmahl, G., Rudolph, D., and Guttmann, P. (1988) "Phase Contrast X-Ray Microscopy—Experiments at the BESSY Storage Ring", in Micro 2, p. 228–232.

Soret, J. L. (1875) "Über die durch Kreisgitter erzeugten Diffractionsphänomene" *Ann. Phys. Chem.*, Vol. **156**, p. 99–113.

Vladimirsky, Y., Attwood, D. T., Kern, D. P., Chang, T. H. P., ADE, H., Jacobsen, C., Kirz, J., McNulty, I., Rosser, R. J., Rarback, H., Shu, D. (1986) "High Resolution X-Ray Zone Plates", in "Soft X-Ray Optics and Technology" *Proc SPIE*, Vol. **733**, p. 449.

Vladimirsky, Y., Kern, D., Meyer-Ilse, W., and Attwood, D. (1989) "X-Ray Imaging of Nannostructure Patterns", in *Appl. Phys. Lett.* to be published in 1989.

Walker, A. B. C., Barbee, T. W., Hoover, R. B., and Lindblom, J. F. (1988): "Soft X-Ray Images of the Solar Corona with a Normal Incidence Cassegrain Multilayer Telescope" to be published in Science, revised July 1988.

Zernike, F. (1935): "Das Phasenkontrastverfahren bei der mikroskopischen Betrachtung", *Zeitschr. f. Techn. Physik*, Nr. **11**, p. 454–457.

DISCUSSION

Q.   Have you considered cooling biological specimen to reduce radiation damage?
(Howard, C. V.)

A.   We have thought about it, but postponed it, because it is very difficult to realize. The main difficulties are as follows:
Once the object is cooled down and has been transferred to the vacuum vessel of the x-ray microscope, the object must be surrounded by a chamber which is at lower temperature than the object. Otherwise the object will trap the residual gases and will be contaminated most effectively, mainly by water vapour which will form ice crystals. As the distance of the microzone plate to the object is in the order of 1 mm, a very sophisticated design has to be developed to separate the microzone plate from the cooled components to avoid the objects contamination. Existing cryo transfer systems, which sometimes are restricted to vertically mounted electron microscopes, whereas our x-ray microscopes are horizontally mounted, can not be used. Therefore new cryo transfer systems from air pressure to vacuum, which meet the technical requirements of x-ray microscopes have to be developed.

Q.   What is the optical depth of field in x-ray microscopy? Is it always larger than the specimen thickness? If so, then stereoscopic images can only be obtained as projection images with various specimen orientations. (Brakenhoff, G. J.)

A.   The geometrical optical depth resolution of a zone plate is given by Eq. (8). For MZP3, which is the zone plate with the highest resolution at the Göttingen XM, it results in 1.69 μm when imaging with $\lambda=4.5$ nm. Of course it depends on the object whether the thickness of the object exceeds the depth resolution of the zone plate or not. Objects, which are investigated in x-ray microscopy, are in general thicker than the focal depth of the zone plate, so that stereo pairs can be calculated by the well known optical sectioning methods.

Q.   How will the phase plate in x-ray microscopy affect the fidelity of imaging, or to put it differently the "optical transfer function"?   (Brakenhoff, G. J.)

A.   In the phase contrast mode it is necessary to use quasi-coherent parallel illumination together with a phase plate in the back focal plane. In our first experiments this situation was only approximated (see Fig. 6). Up to now we did not analyse the optical transfer function of the system. Nevertheless, as a phase plate always shows absorption for soft x-radiation, a situation between the phase contrast mode and the dark field mode is given. If we approach the quasi-coherent illumination with an improved optical setup (see Fig. 8), we can use a phase plate of smaller diameter and thus also small spatial frequencies will contribute to the phase contrast image.